Journal of Chromatography, 312 (1984) 31–47
Elsevier Science Publishers B.V., Amsterdam — Printed in The Netherlands

CHROM. 17,033

USE OF ELECTRON-CAPTURE DATA AT SHORT PULSE INTERVALS FOR STUDY OF ELECTRON-CAPTURE MECHANISMS

NICOLAS HERNANDEZ-GIL and W. E. WENTWORTH*
Chemistry Department, University of Houston, UP, 4800 Calhoun Street, Houston, TX 77004 (U.S.A.)
and
T. LIMERO and E. C. M. CHEN
School of Science and Technology, University of Houston, CL, Houston, TX 77058 (U.S.A.)
(First received November 3rd, 1983; revised manuscript received April 18th, 1984)

SUMMARY

Electron-capture data obtained at short pulse intervals (50–100 μsec) can be used to determine electron-capture mechanisms. The response function has been derived and it differs considerably from that at steady-state conditions. The electron-capture coefficient can be defined from the response function and it is directly proportional to the pulse frequency. The derived response function is in agreement with the experimental concentration, temperature, and pulse interval dependence. The response is independent of pulse width providing short pulse widths (0.5–1.0 μsec) are used at intervals larger than 50 μsec. The electron-capture coefficient at short pulse intervals is lower than at long pulse intervals where steady-state conditions prevail. However, this is partially compensated by a greater standing current at short pulse intervals.

INTRODUCTION

The use of the electron-capture detector to obtain fundamental rate constants and electron affinities has been described using data at long pulse intervals and steady-state conditions[1]. The purpose of this paper is to describe the use of electron-capture data at short pulse intervals to obtain similar fundamental information. Experimental data are presented to support the kinetic analysis. Both the concentration and temperature dependence are presented for both non-dissociative and dissociative capture mechanisms. The use of data at short pulse intervals has the advantage of a higher standing current and consequently a greater signal-to-noise level. Not only is the electrical noise decreased, but also the baseline appears to be less sensitive to impurities in the carrier gas. However, the response at short pulse intervals is considerably lower than at steady-state conditions.

In recent years Aue and co-workers[2,3] have studied the mechanism of direct-current electron capture. They propose that the response is due to enhanced

0021-9673/84/$03.00

electron–positive ion recombination as a result of the space charge created by the migration of anions towards the anode. With this mechanism they can account for hypercoulometric responses observed with direct-current electron capture. They claim that "classical theory does not allow for hypercoulometric response...". Presumably the basic kinetic mechanism presented in this paper and previous works, as described in the review by Pellizzari[4], is referred to as the classical theory. This classical theory dates back to the sixties and was applied specifically to the pulsed mode where the time between pulses is sufficiently great as to establish steady-state conditions. Steady state for a ^{3}H electron-capture detector is >1000 μsec and for ^{63}Ni it is in excess of 2000 μsec. Whether these conditions are typical of commercial electron-capture detector operating conditions is another matter. The reason for steady-state conditions was to simplify the mathematical analysis. These conditions for the pulsed mode also give electron attachment and subsequent reactions the opportunity to occur under field-free conditions. The resulting steady-state electron concentration is analyzed by pulsing out the electrons with a pulse of the shortest duration so as to minimize the opportunity of electron attachment under the influence of the pulse. The fundamental assumption being that the extent of electron attachment under the 1000–2000 μsec field-free period will far exceed the attachment that may occur during the brief 0.5–2 μsec pulse. This objective is in great contrast to the direct-current mode whereby the attachment process occurs while the electron is drifting toward the anode under the influence of a field. Obviously the so-called classical theory cannot account for electron attachment in the direct-current mode.

More recently Aue and Siu[5] presented evidence for more than one response mechanism in pulsed electron-capture detectors. They examined the electron-capture response in the pulsed mode but with varying pulse widths up to 20 μsec. One response occurred at short pulse widths on the order of 2 μsec at a potential of 30 V while another occurred at pulse widths of *ca.* 10 μsec. Special note should be made that the response at longer pulse widths diminishes as the pulse potential and the pulse interval are increased. It would appear that the pulse mode at pulse intervals of 1000 to 2000 μsec and pulse widths of 2 μsec at 30 V would lead to a single mechanism. This would logically be attributed to the reaction during the field-free conditions. Furthermore, when argon–methane (90:10) is used as the carrier gas the electron mobility is greater and the electrons can be collected in 0.5 μsec at 30 V and the effect of reaction during the applied pulse is further minimized.

Aue and co-workers[2,3,5] designed an electron-capture cell so that the electron-capturing sample enters in a region separated from the ionization region. The purpose of this experiment was to demonstrate that electron capture can occur without the necessity of the positive ions. According to Aue and co-workers[2,3,5], "the separated mode prevents the contact of cations with solute derived anions, thereby precluding the classical neutralization mechanism". There are several points to be made concerning these experiments and the resulting conclusions. First, the negative ion–positive ion recombination only plays a role in the electron-capture mechanism when the anion can thermally undergo electron detachment, *i.e.* the capturing species has a low electron affinity. For all other electron-attachment mechanisms the anion–cation reaction rate constant does not enter in the final expression for the capture coefficient[6]. A compound such as acetophenone, which has an electron affinity of 0.33 eV, should be examined in these experiments to test the significance of the

anion–cation recombination rate constant. Neither lindane nor 2,4,6-trinitrotoluene would form anions which could undergo thermal detachment.

The second point to be made concerns the distribution of positive ions within the electron-capture detector. Aue and Kapila[2] have concluded that the "centre-of-charge lies about 1 mm from the ^{63}Ni foil (in nitrogen at ambient temperature and pressure)". The distribution of ion pairs produced initially by the β-emission must certainly be greatest at the surface of the foil and decrease continuously with the distance away from the foil. Precisely how the centre-of-charge is defined with respect to this distribution was not given. Grimsrud and Connolly[7] have also experimentally measured the positive ion density using an atmospheric pressure ionization mass spectrometer. They indeed do observe a rapid decrease in ion density as the distance between the radioactive foil (in the shape of a disk) and the aperture to the mass spectrometer is increased. However, when these results are used in predicting the ion density in a cylindrical electron-capture detector configuration the ion density within the cell (10 mm diameter and 20 mm length) does not fall off dramatically as the distance from the foil is increased. For argon–methane carrier gas at one atmosphere pressure and 200°C the ion density at the center of the cell is only 0.66 as great as the density 0.5 mm from the wall. Furthermore, the ion density beyond the end of the cylinder remained high, *e.g.* at 10 mm from the end of the radioactive foil the ion density is about 0.20 as great as at the center of the cell. Applying these results to the cell design by Aue and co-workers[2,3,5], it is questionable whether the positive ions are separated from the region where the electron-capturing species enters the cell.

Finally a comment concerning the negative ion–positive ion recombination rate constant is appropriate. Pellizzari[4] stated that "recombination of ions occurs 10^5–10^8 times faster than the recombination of free electrons and positive ions". The recombination rate for negative ions may exceed that for electrons but it is very doubtful that it is much larger and it is not necessary in order for the proposed kinetic model[4] to account for electron capture. In an earlier study Wentworth *et al.*[8] estimated the negative ion–positive ion recombination rate constant to exceed that for the electrons by approximately a factor of eight for a study of some aromatic hydrocarbons. This value cannot be determined very precisely by this experiment and furthermore should vary somewhat for different anions as well as cations. In any event the recombination rate constants for negative ions should be on the same order of magnitude as that for electrons and this is quite satisfactory for the kinetic model to account for electron capture. As mentioned previously, this rate constant is included in the electron-capture coefficient only when non-dissociative capture occurs to a molecule with a sufficiently low electron affinity that the electron can be detached at thermal energies. Even in this case a more detailed kinetic analysis[9] reveals that the fate of the negative ion is not restricted to recombination with positive ions. Following the application of the brief pulse to collect electrons, the negative ion will re-equilibrate and in so doing may detach electrons which are in excess of those being produced by the β-particles. This results in an excess of electrons which enhances the rate of electron–positive ion recombination. Of course even in this mechanism it is important to have positive ions for the electron recombination.

KINETIC ANALYSIS

The kinetic model for electron capture that has been presented elsewhere[6,8,10] is summarized in the following reaction sequence

$$\beta + (\mathrm{Ar} + 10\%\ \mathrm{CH_4}) \xrightarrow{k_p R_\beta} \mathrm{e^-} + \oplus + \beta^* \tag{1}$$

$$\mathrm{e^-} + \oplus \xrightarrow{k'_D} \text{neutral species} \tag{2}$$

$$\mathrm{e^-} + \mathrm{AB} \xrightarrow{k_{12}} \mathrm{A} + \mathrm{B^-} \tag{3}$$

$$\mathrm{e^-} + \mathrm{AB} \xrightarrow{k_1} \mathrm{AB^-} \tag{4}$$

$$\mathrm{AB^-} \xrightarrow{k_{-1}} \mathrm{AB} + \mathrm{e^-} \tag{5}$$

$$\mathrm{AB^-} \xrightarrow{k_2} \mathrm{A} + \mathrm{B^-} \tag{6}$$

$$\mathrm{AB^-} + \oplus \xrightarrow{k'_{N1}} \text{neutral species} \tag{7}$$

$$\mathrm{B^-} + \oplus \xrightarrow{k'_{N2}} \text{neutral species} \tag{8}$$

where AB represents any polyatomic molecule capable of capturing or attaching an electron, β^* designates the β-particle with reduced energy as a result of ion pair formation and the k's are standard kinetic rate constants. The rate constant $k_p R_\beta$ represents the overall rate of ion pair formation, while $\oplus$ represents a positive ion.

The three temperature regions in terms of the relative magnitude of the rate constants[6] can be designated corresponding to three mechanisms

$$\alpha\text{: } k_{-1} > k'_{N1}[\oplus] > k_2$$

$$\beta\text{: } k'_{N1}[\oplus] > k_{-1} > k_2$$

$$\gamma\text{: } k_{-1} > k_2 > k'_{N1}[\oplus]$$

If the electron-attachment process produces $\mathrm{AB^-}$ and does not detach according to reaction 5, then it is impossible to differentiate kinetically between reactions 3 and 4 in terms of electron capture. Mechanism β encompasses both dissociative electron capture and non-dissociative capture to compounds with high electron affinities. Generally, reactions 3 and 4 differ in that reaction 3 can have a significant activation energy, whereas for reaction 4, the activation energy is generally small.

In an earlier analysis of this kinetic model[8], the postive-ion concentration was assumed to build up to a constant value and furthermore, that it did not change

significantly when the electron-capturing species is present. However, it was shown in a later analysis[9] that the positive-ion concentration decreases at the same time that the electron concentration decreases. The differential equations describing the change in concentration of the various species between pulses were solved numerically bringing into consideration the variation of the positive-ion concentration[9].

Steady-state conditions

The following expressions for the capture coefficients at steady state, K_∞, were derived[9].

For the β-mechanism

$$\frac{b^2 - [e^-]^2}{b\,[e^-]} = (K_\infty)_\beta[AB] \tag{9}$$

where

$$(K_\infty)_\beta = \frac{k_1}{k_D} \tag{10}$$

For the α-mechanism

$$\frac{b^2 - [e^-]^2}{[e^-]^2} = (K_\infty)_\alpha[AB] \tag{11}$$

where

$$(K_\infty)_\alpha = \frac{k_1 k'_{N1}\,[\oplus]}{k_{-1}k_D} \tag{12}$$

For the γ-mechanism

$$\frac{b^2 - [e^-]^2}{b[e^-]} = (K_\infty)_\gamma[AB] \tag{13}$$

where

$$(K_\infty)_\gamma = \frac{k_1 k_2}{k_{-1}k_D} \tag{14}$$

k_D is defined as

$$k_D = k'_D\,[\oplus_0] \tag{15}$$

where $[\oplus_0]$ is the positive ion concentration and b is the electron concentration in the absence of electron-capturing species.

It should be pointed out that in order to evaluate k_1 (β-mechanism) under steady-state conditions, k_D must be determined at the same time[13]. The values of k_D are calculated by measurement of the standing current in the electron-capture detec-

tor as a function of the time between pulses, t_p[8]. It is assumed that the carrier gas is pure and k_D is simply a measure of the electron–positive ion recombination rate. However, if impurities are present, their effect on the attachment rate is generally, as impurities themselves, unknown.

Linear region conditions

At short pulse intervals the general derivation can be carried out along the same procedures as that for the β-mechanism[14]. Since the rate of electron production is constant at short pulse intervals the electron concentration increases linearly and we refer to this as the "linear region". The differential rate expressions in the linear region reduce to

$$\frac{db}{dt} = k_p R_\beta \tag{16}$$

$$\frac{d\,[e^-]}{dt} = k_p R_\beta - k_1[e^-]\,[AB] + k_{-1}[AB^-] - k_{12}[e^-]\,[AB] \tag{17}$$

$$\frac{d\,[AB^-]}{dt} = k_1\,[e^-]\,[AB] - k_{-1}\,[AB^-] - k_2\,[AB^-] - k'_{N1}\,[\oplus]\,[AB^-] \tag{18}$$

Assuming steady state for $[AB^-]$, eqn. 18 can be set to zero and solved for $[AB^-]$

$$[AB^-] = \frac{k_1\,[e^-]\,[AB]}{k_{-1} + k_2 + k'_{N1}\,[\oplus]} \tag{19}$$

Substitution into eqn. 17 gives

$$\frac{d\,[e^-]}{dt} = k_p R_\beta - H\,[e^-] \tag{20}$$

where

$$H = \left\{k_{12} + \frac{k_1(k_2 + k'_{N1}\,[\oplus])}{k_{-1} + k_2 + k'_{N1}\,[\oplus]}\right\}[AB] \tag{21}$$

Integration of eqn. 21 gives

$$\frac{-1}{H} \ln \frac{k_p R_\beta - H[e^-]}{k_p R_\beta} = t_p \tag{22}$$

that yields

$$[e^-] = \frac{k_p R_\beta}{H}\,[1 - \exp\,(-Ht_p)] \tag{23}$$

Eqn. 23 is simplified by expanding the exponential term into a MacLaurin's series

$$[e^-] = k_p R_\beta t_p \left(1 - \frac{H t_p}{2!} + \ldots\right) \tag{24}$$

Neglecting higher terms than the second term and substituting b from the integral of eqn. 16, $b = (k_p R_\beta)(t_p)$, we obtain

$$\frac{b - [e^-]}{b} = \frac{H}{2} t_p \tag{25}$$

Substituting for H from eqn. 21

$$\frac{b - [e^-]}{b} = \left\{k_{12} + \frac{k_1(k_2 + k'_{N1}[\oplus])}{(k_{-1} + k_2 + k'_{N1}[\oplus])}\right\} \frac{t_p}{2} [AB] = K[AB] \tag{26}$$

where K is the capture coefficient. Eqn. 26 differs from the general solution at steady state in the $t_p/2$ factor and the absence of $1/k_D$.

For the α-mechanism $k_{12} = k_2 = 0$ and $k_{-1} \gg k'_{N1}[\oplus]t_p$ and eqn. 26 becomes

$$\frac{b - [e^-]}{b} = \frac{k_1 k'_{N1}[\oplus] t_p}{2k_{-1}} [AB] \tag{27}$$

or

$$\frac{b - [e^-]}{b} = K_\alpha [AB] \tag{28}$$

where

$$K_\alpha = \frac{k_1 k'_{N1}[\oplus]}{2k_{-1}} t_p \tag{29}$$

K_α is the capture coefficient for the α-mechanism at high temperature in the linear region.

Substituting the statistical mechanical expression for the thermodynamic equilibrium constant[8] into eqn. 28 and taking logarithms we obtain

$$\ln K_\alpha T^{3/2} = \ln \left\{\frac{k'_{N1}[\oplus] t_p}{2} A\right\} + \frac{EA}{RT} \tag{30}$$

where A is the pre-exponential factor, EA is the electron affinity of the molecule and R is the ideal gas constant. If $k'_{N1}[\oplus]$ is temperature independent, the EA of a molecule can be determined from the graph of $\ln K_\alpha T^{3/2}$ *versus* T^{-1}.

At low temperatures $k'_{N1}[\oplus] \gg k_{-1}$. Eqn. 28 becomes

$$\frac{b - [e^-]}{b} = \frac{k_1}{2} t_p [AB] \tag{31}$$

The electron attachment rate constant, k_1, can be determined directly from the slope of a graph $\frac{b - [e^-]}{b}$ *versus* [AB] without knowing [⊕] or k_D. An accurate measurement of t_p is needed.

The activation energy for electron attachment (E^*) can be determined from the slope of a graph ln $[(1/2)\, k_1 t_p T^{3/2}]$ *versus* T^{-1} (ref. 14).

EXPERIMENTAL

The electron-capture measurements were carried out using a modified Varian Aerograph gas chromatograph. A 25 × 0.32 mm I.D. fused-silica glass capillary column with bonded methylphenyl silicone from Quadrex Corporation was used. Samples were injected directly on column with a 5-μl Hamilton 75-SN syringe (32 gauge, 12 cm in length) through an on-column injector[15] that utilizes a 25-gauge syringe needle to make the septum penetration and to act also as the protective guide for the finer sampling needle. The injector block was not heated. In order to prevent sample loss from the needle, 1 μl of air was pulled into the syringe after the desired sample size had been introduced to the syringe. In order to test the sampling technique different sample sizes of a $5 \cdot 10^{-3}$ (v/v) benzylmethyl ether solution in toluene were run using the flame ionization detector. These concentrations are generally higher than for the electron-capture measurement, so overloading effects would be more likely with the flame ionization measurements. However, a graph of peak height from the flame ionization detector *versus* sample size was linear with a zero intercept, indicating that no overloading occurred and that the injection procedure was quantitative.

A Data Pulse 102 square-wave pulse generator was used to pulse the electron-capture detector. A combination of pulse width and potential was used so that all electrons were collected. The pulse was measured using a Tektronix 2215 oscilloscope. The electron-capture current was measured with a Keithly 417 picoammeter or an electrometer constructed in the lab using a Philbrick Research SP2A operational amplifier and recorded on a Houston Instrument strip chart recorder.

The flame ionization detector was used to identify the major component and was run in parallel with the electron-capture detector. Once suitable chromatographic conditions had been achieved, the gas chromatographic column was connected directly to the electron-capture detector for quantitative measurements.

The electron-capture detector was electrically insulated from the aluminum heating block using a piece of pyrex tubing. The temperature of the electron-capture detector was controlled with a Valco ITC-K12 temperature controller. The heat was supplied by two cartridge heaters inserted in the aluminum block. The temperature was measured using a mercury thermometer with 1°C-divisions and a thermocouple using a Doric 400A digital display. The electron-capture detector employing 15 mCi ^{63}Ni and 150 mCi scandium tritide foils were of cylindrical geometry[16] whereas titanium tritide was used in a parallel plate type geometry. The ^{63}Ni and scandium

tritide electron-capture detector had an internal diameter of 1.4 cm. The ^{63}Ni and scandium tritide foils were in contact with the cylinder wall and received the negative pulse. The cathode was a 1/16 in. rod at the center of the cylinder. For the scandium tritide detector the cathode extended through the cylinder within the ionization region. However, due to the greater range for the β's in the ^{63}Ni detector, the electrode was retracted to the edge of the foil so as to minimize direct interaction with the β-particles and collection of charge during the pulse free period.

Nitrogen (ultra high purity) from Matheson was used as carrier gas when the flame ionization detector was in operation. For the quantitative electron-capture measurements argon–methane (90:10) from Big Three Welding (<5 ppm O_2) was used as the carrier gas after filtering with a 5 Å molecular sieve trap. Typical flow-rates were 5 ml/min through the column and 140 ml/min as scavenger added between the column and the electron-capture detector.

The areas under the chromatographic peaks were obtained by the trapezoid method of numerical integration.

Spectrophotometric grade dichloromethane (Aldrich), reagent grade biacetyl (Eastman Organic Chemicals), and hexafluorobenzene >99% (Aldrich) were used. Solutions were prepared in nanograde hexane (Mallinckrodt) except for biacetyl which were prepared in nanograde toluene (Mallinckrodt). All the solvents were checked for electron-capturing impurities and coelution with the compound of interest.

In order to obtain a critical evaluation of the concentration dependence a thermal conductivity detector was used to measure the relative concentration of the component being chromatographed. For these experiments the gas stream from a Gow Mac gas chromatograph was split between a thermal conductivity detector and the electron-capture detector using restrictors so that the majority of the flow was towards the thermal conductivity detector. The thermal conductivity detector response at the peak maximum was assumed to be directly proportional to the concentration and the corresponding electron capture detector response at the peak maximum was evaluated. This procedure eliminates effects due to peak broadening and inaccuracies in sample injection.

RESULTS AND DISCUSSION

Concentration dependence

As a test of the kinetic model for electron-capture mechanisms using data at short pulse intervals, the concentration dependence was investigated extensively. An approximate expression for the concentration dependence of the electron-capture detector response was given in eqns. 25 and 26 where the extent of capture was low (<15%). In order to test the model over a greater extent of capture, eqns. 22–24 or some modification of these must be used. Using $b = (k_p R_\beta)(t_p)$, eqn. 24 can be written in terms of a series

$$\frac{b - [e^-]}{b} = \frac{Ht_p}{2!} - \frac{(Ht_p)^2}{3!} + \frac{(Ht_p)^3}{4!} - \cdots \tag{32}$$

From eqns. 25 and 26 $Ht_p = 2K[AB]$ and the series can be written as

$$\frac{b - [e^-]}{b} = \frac{2K[AB]}{2!} - \frac{(2K[AB]^2)}{3!} + \ldots$$

A graph of $\frac{b - [e^-]}{b}$ *versus* concentration in units of (K^{-1}) is shown in Fig. 1. One can see the deviation from linearity at about 15% capture. The experimental data for tetrachloromethane are also shown in Fig. 1 and the good agreement with the calculated curve is obvious.

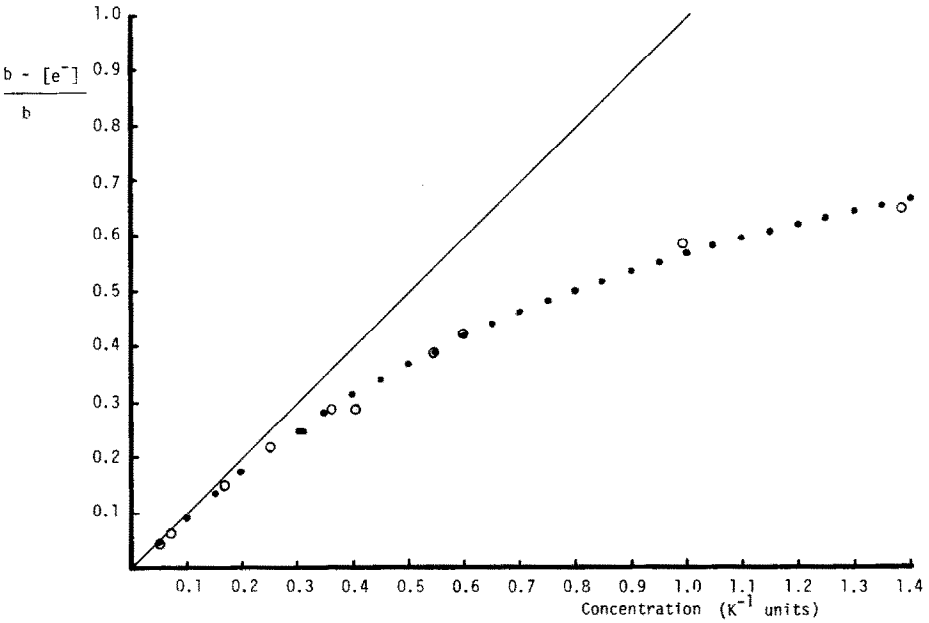

Fig. 1. Electron-capture response as a function of concentration. O, Data points for tetrachloromethane.

The response curve shown in Fig. 1 deviates markedly from the linear function at high concentrations. The response increases very slightly with increasing concentration at concentrations where the percent capture exceeds ~60%. This is observed experimentally since it is very difficult to obtain complete capture of the electrons using short pulse intervals.

In order to test the concentration dependence more critically, the gas chromatographic effluent was split so that the relative concentration could be measured directly on a thermal conductivity detector. The data were tested rigorously by carrying out a non-linear least squares adjustment to eqn. 22 which was slightly rearranged for convenience using $b = (k_p R_\beta)(t_p)$.

$$-\ln \frac{b - H[e^-]t_p}{b} = Ht_p \tag{33}$$

Substituting for H from eqn. 21 and K from eqn. 26

$$-\ln \frac{b - 2K\,[\mathrm{AB}]\,[\mathrm{e}^-]}{b} = 2K\,[\mathrm{AB}] \tag{34}$$

Since the relative concentration of AB was measured by the thermal conductivity detector (TCD) response, R_{TCD},

$$R_{\mathrm{TCD}} = K_{\mathrm{TCD}}\,[\mathrm{AB}] \tag{35}$$

eqn. 34 becomes

$$-\ln \frac{b - \frac{2K}{K_{\mathrm{TCD}}}(R_{\mathrm{TCD}})\,[\mathrm{e}^-]}{b} = \frac{2K}{K_{\mathrm{TCD}}}(R_{\mathrm{TCD}}) \tag{36}$$

The measured quantities at each concentration are then R_{TCD}, $[\mathrm{e}^-]$, b and the adjustable parameter is simply $\left(\frac{2K}{K_{\mathrm{TCD}}}\right)$. In order to show the least squares adjustment to eqn. 36 a graph of the left-hand-side of eqn. 36 *versus* R_{TCD} is shown in Fig. 2 for sulfur dioxide. The percent capture is shown on the right-hand-scale and it should be noted that there are relatively small changes in percent capture for the larger values. Consequently the errors in the linearized function at high electron capture

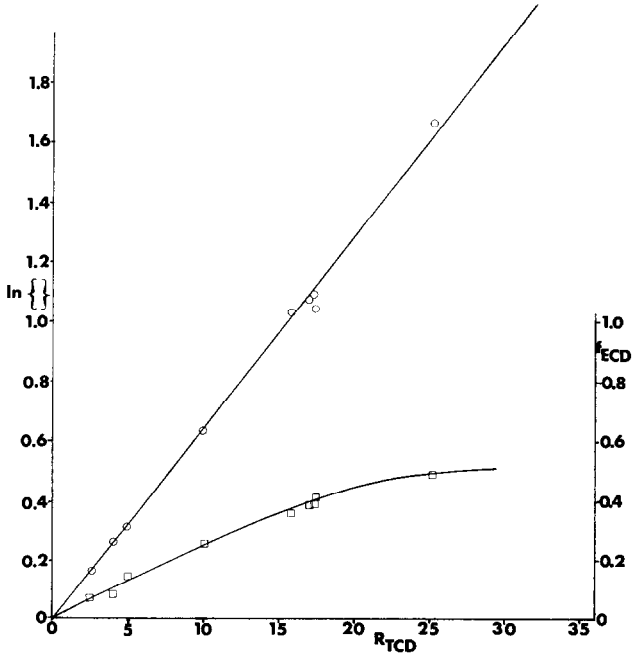

Fig. 2. Linearized response for sulfur dioxide. ln { } is defined in eqn. 36; R_{TCD} = thermal conductivity detector response. ○, ln { } *versus* R_{TCD}; □, fraction of electron capture (f_{ECD}) *versus* R_{TCD}.

are much greater than for the smaller values. In fact the errors appear to be intolerable when the extent of capture exceeds 50%.

Sulfur dioxide captures electrons non-dissociatively and Fig. 2 shows how eqn. 33, as modified in eqn. 36, adequately represents the linearized electron-capture detector response. In order to show how the same equations can represent electron-capture detector response for dissociative electron capture, the same type graphs are shown for dichloromethane in Fig. 3. Again the linearized function is adequately obeyed up to ~50%.

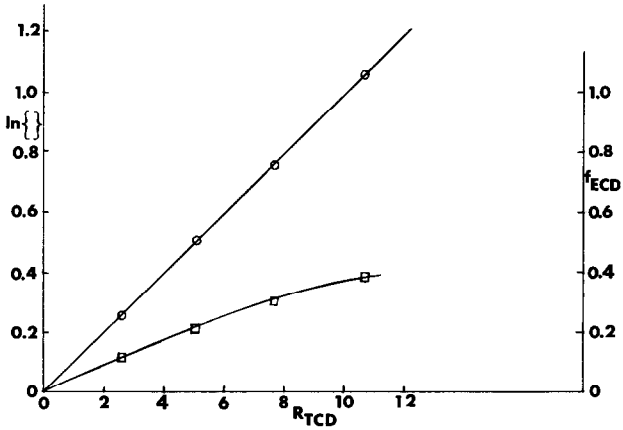

Fig. 3. Linearized response for dichloromethane. ln { } is defined in eqn. 36; R_{TCD} = thermal conductivity detector response. ○, ln { } *versus* R_{TCD}; □, fraction of electron capture (f_{ECD}) *versus* R_{TCD}.

Temperature dependence

In order to further test the derived response function shown in eqns. 21 and 22, we have examined the temperature dependence for different attachment mechanisms and types of detectors. Generally concentrations were kept low enough so that eqn. 26 could be used to calculate the capture coefficient K. If the percent capture exceeded 15% the correction was made from the higher order terms in eqn. 32 or the exact expression in eqn. 34.

Hexafluorobenzene (C_6F_6) was chosen to represent the mechanism involving stable negative ion formation ($C_6F_6^-$) which has been identified as such using an atmospheric pressure ionization mass spectrometer. Both the α and β temperature regions are observed, corresponding to eqns. 28–31. Hexafluorobenzene was run using an electron-capture detector with a tritium foil and parallel plate geometry as shown by the solid stars in Fig. 4. This data is primarily in the β-region but at high temperatures the capture coefficient decreases characteristic of the α-region. The data for hexafluorobenzene using a ^{63}Ni electron-capture detector and concentric geometry are consistent with the parallel plate detector in the α-region as shown by the open stars in Fig. 4. However, using the ^{63}Ni electron-capture detector, results could be obtained at higher temperatures than with tritium. Hexafluorobenzene data were also obtained with tritium as scandium tritide in a detector with cylindrical geometry and nitrogen as the carrier gas. These data are represented by open stars in dark

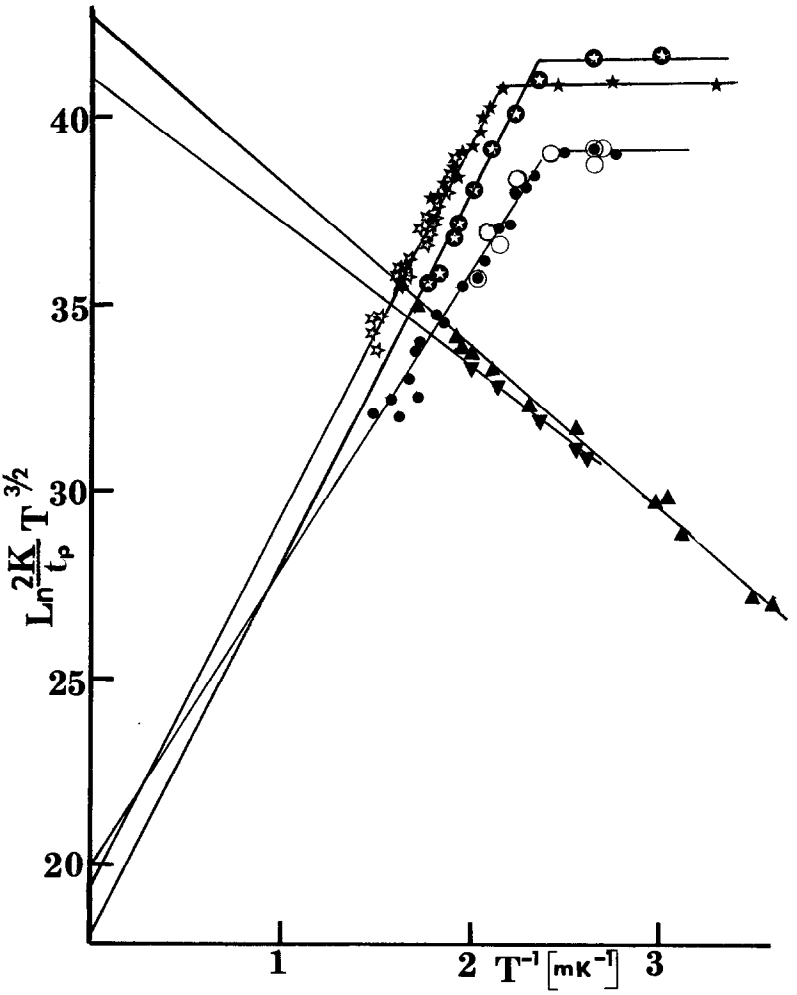

Fig. 4. Temperature dependence of electron capture coefficient (K); K defined by eqn. 26. ★, hexafluorobenzene using tritium in parallel plate geometry; ☆, hexafluorobenzene using ^{63}Ni in cylindrical geometry; ✪, hexafluorobenzene using scandium tritide in cylindrical geometry; ●, biacetyl using ^{63}Ni; ○, biacetyl using scandium tritide; ▲, dichloromethane using ^{63}Ni; ▼, dichloromethane using scandium tritide.

circles in Fig. 4. Note that the data in the α-region have a slope parallel to that obtained with argon–methane (90:10) as carrier gas. The lower values in the α-region suggest that nitrogen has a lower k_N value. This is consistent with the greater range of the β-particles in nitrogen and a more diffuse positive ion distribution. There is no good explanation for the larger response in the β-region except that it may be due to a slight difference in electron energy distribution coming from tritium compared to ^{63}Ni (ref. 14).

Biacetyl also undergoes non-dissociative electron attachment and data obtained with both ^{63}Ni and scandium tritide electron-capture detector are also shown

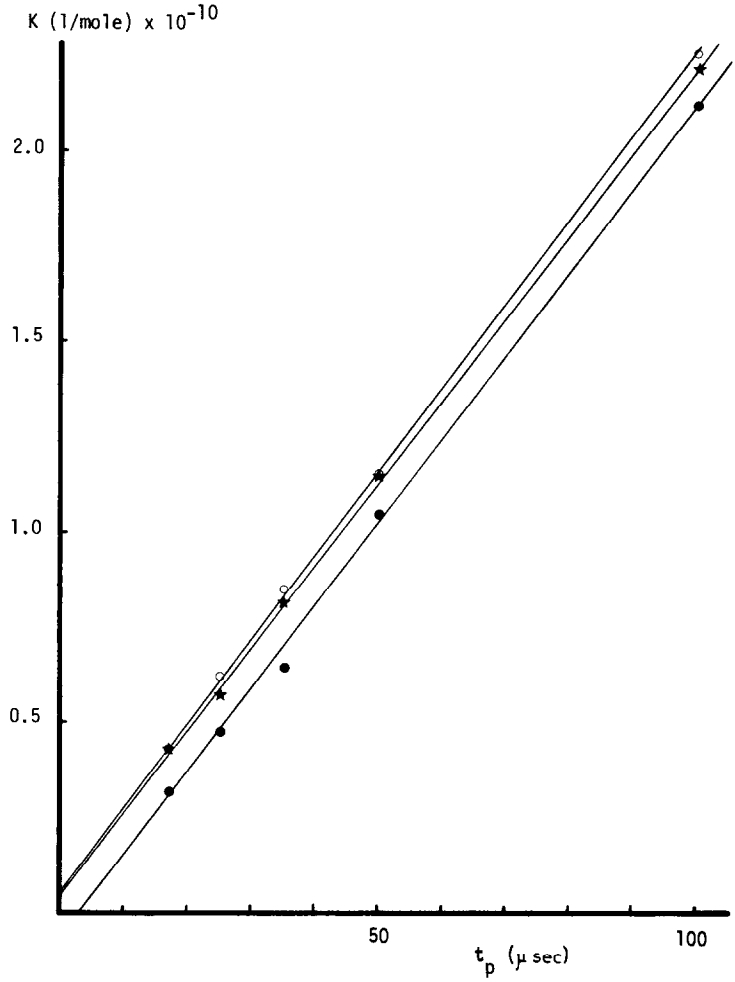

Fig. 5. Capture coefficient (*K*) *versus* pulse interval for tetrachloromethane at 100°C. ○, argon–methane (90:10); ★, helium–[argon–methane (90:10)] (9:91); ●, helium–[argon–methane (90:10)] (17:83). Pulse width = 1 μsec.

in Fig. 4. The data is primarily in the α-region and the data from both detectors are consistent. However, there are three higher temperature data points from the scandium tritide electron-capture detector which fall considerably below the straight line[17]. These are not shown in Fig. 4 and there is no apparent explanation for their deviation.

Also shown in Fig. 4 are data for dichloromethane which undergoes dissociative electron attachment. The data give a characteristic negative slope related to the activation energy for the process. The ^{63}Ni data are over a much greater temperature range and define the slope more precisely. The tritium data appear to give a slightly lower slope but the difference is barely outside the expected errors. The magnitudes of both sets of data are certainly consistent.

Dependence on pulse interval

The general expression for the capture coefficient as given in eqn. 26 is directly related to the pulse interval t_p. In order to further test the model for the linear region (short pulse intervals), the capture coefficient for tetrachloromethane has been obtained as a function of t_p. Such data are shown in Fig. 5 for tetrachloromethane at 100°C. Note that all three sets of data represent reasonably good straight lines. According to eqn. 26 the capture coefficient should be zero at $t_p = 0$. However, some capture could occur during the 1-μsec pulse width and this would account for a small positive intercept. For the data with 17% helium plus argon–methane the negative intercept could not be explained on this basis and we know of no alternative explanation except experimental error.

The capture coefficient K, as defined in eqn. 26, contains the factor t_p. Since the response function as expressed in eqn. 34 contains the product K [AB], the response function contains t_p and [AB] as the product t_p [AB]. In other words a given response or electron-capture detector current depends upon the simple t_p [AB] product. This is consistent with the constant current mode of electron-capture detector linearization whereby the current is maintained constant by varying the pulse frequency. Since t_p is the inverse of pulse frequency, the concentration is thus directly proportional to the pulse frequency. Since eqn. 34 applies to any electron-capture mechanism, the concentration–pulse frequency relationship should be satisfied for all modes of capture providing the frequency is in the linear region.

Dependence on pulse width

Under normal operating conditions the pulse width is quite small, typically 0.5–1.0 μsec for argon–methane and 2 μsec for nitrogen, compared to the pulse interval. Consequently the extent of reaction during the applied pulse is small and can be neglected compared to the reaction at zero voltage between pulses. However, at very short pulse intervals the pulse width can be significant and the reaction during the applied potential can affect the capture coefficient. This effect is shown in Fig. 6 where again the data is for tetrachloromethane at 100°C. The detector contained a ^{3}H foil with parallel plate geometry. From the electron-capture data the rate constant for attachment was calculated by eqn. 31, where $K = \frac{k_1}{2} t_p$. Of course k_1 should be independent of t_p so ideally with no reaction during the applied pulse, the graph of k_1 should be a horizontal line. Note from the curves in Fig. 6 that k_1 appears to be constant at short pulse widths of 0.5 and 1 μsec. At 2-μsec pulse widths some deviation is noted at short pulse intervals < 50 μsec. At 5-μsec pulse width the deviation is very significant below 50-μsec pulse intervals. Of course from a practical stand point a pulse width of 1 μsec at 40 V is generally sufficient to collect all free electrons and there is no need to use pulse widths as great as 5 μsec. A similar curve at a pulse width of 5 μsec was determined using a ^{63}Ni detector. Similar data was also obtained using a detector with scandium tritide in a concentric geometry and in a pin-in-cup geometry where the center electrode is pulled out to the edge of the radioactive foil. Different shaped curves were observed depending upon the geometry of the electron-capture detector[17]. However, at pulse intervals in excess of 50 μsec and pulse widths of 0.5–1.0 μsec k_1 was constant. Negative as well as positive deviations can be observed. The negative deviations were most pronounced with the pin-in-cup ge-

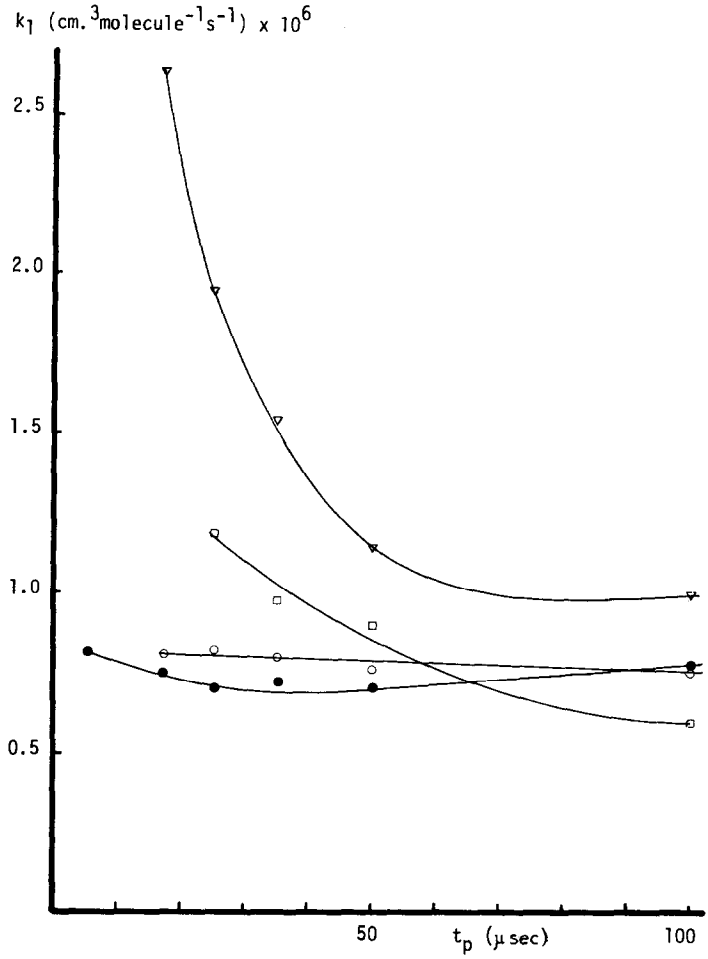

Fig. 6. Electron attachment rate constant measured using different pulse widths. Tritium electron-capture detector with parallel plate geometry. Pulse widths: ●, 0.5 μsec; ○, 1.0 μsec; □, 2.0 μsec; ▽, 5.0 μsec.

ometry at short intervals. In any event the results indicate that at pulse intervals in excess of 50 μsec and short pulse widths $\leqslant 1$ μsec the results should obey the derived response functions, eqns. 21 and 22, or simplified forms in eqns. 26, 27 and 31.

CONCLUSIONS

The electron-capture detector can be operated at short pulse intervals (50–100 μsec) as well as steady-state conditions to study electron-capture mechanisms. A mathematical expression has been derived to describe the response using data at short pulse intervals. The dependence of the capture coefficient on concentration, temperature and pulse interval has been demonstrated with experimental data and this is in agreement with the derived mathematical expression for the response. The capture coefficient is independent of pulse width providing short pulse widths of 0.5 to 1.0 μsec at intervals of > 50 μsec are used.

ACKNOWLEDGEMENTS

The authors would like to express their appreciation to the Robert A. Welch Foundation for the financial support for this project (Grant E-095). We are also grateful of the experimental work of Ms. Ela Desai who measured the temperature dependence of hexafluorobenzene using a scandium tritide electron-capture detector with cylindrical (concentric) geometry.

REFERENCES

1 W. E. Wentworth and E. C. M. Chen, in A. Zlatkis and C. F. Poole (Editors), *Electron Capture —Theory and Practice in Chromatography*, Elsevier, Amsterdam, 1981, Ch. 3.
2 W. A. Aue and S. Kapila, *J. Chromatogr.*, 188 (1980) 1.
3 W. A. Aue and K. W. M. Siu, *J. Chromatogr.*, 203 (1981) 237.
4 E. D. Pellizzari, *J. Chromatogr.*, 98 (1974) 323.
5 W. A. Aue and K. W. M. Siu, *J. Chromatogr.*, 239 (1982) 127.
6 W. E. Wentworth and J. C. Steelhammer, *Radiation Chemistry*, Ch. 4, ACS Publications, Washington, DC, 1968; *Advan. Chem. Ser.*, 82 (1968) 74.
7 E. P. Grimsrud and M. J. Connolly, *J. Chromatogr.*, 239 (1982) 397.
8 W. E. Wentworth, E. C. M. Chen and J. E. Lovelock, *J. Phys. Chem.*, 70 (1966) 445.
9 W. E. Wentworth and E. C. M. Chen, *J. Chromatogr.*, 186 (1979) 99.
10 W. E. Wentworth and R. S. Becker, *J. Amer. Chem. Soc.*, 84 (1962) 4263.
11 W. E. Wentworth, in I. I. Damsky and J. A. Perry (Editors), *Recent Advances in Gas Chromatography*, Marcel Dekker, New York, 1971, pp. 105–123.
12 E. P. Grimsrud, S. H. Kim and P. L. Gobby, *Anal. Chem.*, 51 (1979) 223.
13 E. C. M. Chen, R. D. George and W. E. Wentworth, *J. Chem. Phys.*, 49 (1968) 1973.
14 J. A. Ayala, W. E. Wentworth and E. C. M. Chen, *J. Phys. Chem.*, 85 (1981) 3989.
15 F. S. Wang, H. Shanfield and A. Zlatkis, *Anal. Chem.*, 54 (1982) 1886.
16 A. Zlatkis and D. C. Fenimore, *Rev. Anal. Chem.*, 2 (1975) 317.
17 N. Hernandez, *M.S. Thesis*, University of Houston, Houston, 1983.